

pubs.acs.org/ac Article

Graphene-Fiber Microelectrodes for Ultrasensitive Neurochemical Detection

Yuxin Li, Romana Jarosova, Moriah E. Weese-Myers, and Ashley E. Ross*



Cite This: Anal. Chem. 2022, 94, 4803-4812



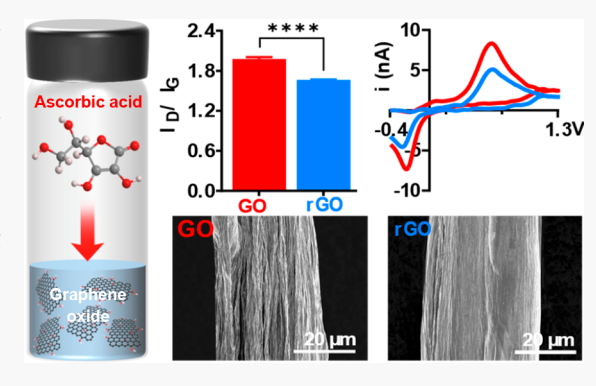
ACCESS

Metrics & More

Article Recommendations

s Supporting Information

ABSTRACT: Here, we have synthesized and characterized graphene-fiber microelectrodes (GFME's) for subsecond detection of neurochemicals with fast-scan cyclic voltammetry (FSCV) for the first time. GFME's exhibited extraordinary properties including faster electron transfer kinetics, significantly improved sensitivity, and ease of tunability that we anticipate will have major impacts on neurochemical detection for years to come. GF's have been used in the literature for various applications; however, scaling their size down to microelectrodes and implementing them as neurochemical microsensors is significantly less developed. The GF's developed in this paper were on average 20–30 μ m in diameter and both graphene oxide (GO) and reduced graphene oxide (rGO) fibers were characterized with FSCV. Neat GF's were synthesized using a one-step dimension-confined hydrothermal strategy. FSCV detection has tradition-



ally used carbon-fiber microelectrodes (CFME's) and more recently carbon nanotube fiber electrodes; however, uniform functionalization and direct control of the 3D surface structure of these materials remain limited. The expansion to GFME's will certainly open new avenues for fine-tuning the electrode surface for specific electrochemical detection. When comparing to traditional CFME's, our GFME's exhibited significant increases in electron transfer, redox cycling, fouling resistance, higher sensitivity, and frequency independent behavior which demonstrates their incredible utility as biological sensors.

■ INTRODUCTION

Here, we have synthesized and characterized graphene oxide (GO) and reduced graphene oxide (rGO) microfibers as microelectrodes for subsecond neurochemical detection. The most popular electrode material for subsecond neurochemical detection is the carbon-fiber microelectrode (CFME), often coupled to fast-scan cyclic voltammetry (FSCV). 1-3 FSCV is an electroanalytical tool used for real-time detection of electroactive neurotransmitters in the brain. 1,4,5 CFME's offer several advantages, most notably their large potential window, stability, and low limits of detection. 1,3,6 Despite these advantages, they remain extremely difficult to uniformly manipulate chemically and structurally due to the inherent heterogeneity of their surface. The ability to tune the carbon surface is highly beneficial for rendering more sensitive surfaces for specific analyte detection and for expanding our fundamental understanding of how analytes interact at various carbon surfaces.

Recently, FSCV has expanded to novel carbon nanomaterials including carbon nanotube (CNT) fibers, $^{7-10}$ carbon nanospikes, $^{11-13}$ and carbon nanohorns, 14,15 due to their excellent electrochemical properties. Carbon nanomaterials have offered significant advances in neurochemical detection due to their high conductivity, large surface area, and geometric crevices on the surface enabling local trapping of neurochemicals on the surface. $^{4,9,12,16-20}$ More specifically,

these carbon nanomaterials have broadened the analytical toolbox available for rapid and sensitive electrochemical detection in tissue. Despite the countless advances these materials provide, very few researchers have adopted these materials in their own laboratories due to inaccessibility to expensive chemical reactors or collaboration with carbon nanomaterial synthesis experts. In addition, purchasing carbon nanotube fibers is much more expensive than carbon fibers. Recently, researchers have demonstrated the importance of considering the 3D structure of the electrode due to geometric effects on electrochemical sensing.²¹ Precisely controlling the 3D macromolecular structure and porosity of the carbon lattice remains challenging on carbon nanotube-based materials. Developing carbon nanomaterials that are more accessible to the broader scientific community while maintaining the excellent electrochemical properties and are easily tunable in their chemical and physical structure would significantly improve electrode design for sensitive biomolecule detection.

Received: December 30, 2021 Accepted: March 2, 2022 Published: March 11, 2022





This paper describes the synthesis and characterization of GO and rGO microfibers for subsecond neurochemical detection. The fiber fabrication can be easily adopted in any research laboratory, fibers have excellent electrochemical properties, and possess a homogeneous surface ripe for chemical and structural tunability.

Graphene is a two-dimensional (2D) material with excellent electronic, mechanical, and thermal properties.²²⁻²⁵ Over the last several years, application of graphene-based materials has grown substantially. 22,24,26-29 Graphene-based materials have been incorporated onto existing electrode substrates to enhance electrochemical detection and have provided unique properties. 19,30,31 Recently, the Gao group used wet-spinning and ion cross-linking to fabricate ultrastrong graphene fibers.3 Several other researchers have synthesized graphene fibers using wet-spinning, hydrothermal methods, as well as microfluidic-assisted assembly. 33-35 GF's are flexible, lightweight, and highly conductive. 28 Using pure graphene-based fibers is advantageous compared to modifying existing electrode substrates with graphene materials because it enables precise electrode-analyte interactions to be studied (without underlying interference from the substrate material). Despite these advantages and to the best of our knowledge, expansion of graphene-based fibers to subsecond electrochemical detection of biomolecules for tissue applications is nonexistent.

A few researchers in FSCV have explored the use of graphene-based material for electrochemical detection of dopamine. In 2020, the Venton group electrodeposited GO onto CFME's surface to enhance detection of dopamine with FSCV.¹⁹ They reported improvements in sensitivity and limits of detection. More recently, the Cui group developed fuzzy graphene microelectrode arrays which also significantly improved detection limits for dopamine.³⁰ Overall, these findings suggest that graphene-based materials are beneficial for electrochemical detection of neurochemicals and supports the need to further develop pure graphene-based materials for biomolecule detection. We have adopted and modified existing hydrothermal methods for synthesizing GO and rGO fibers that are on average 20-30 μ m in diameter for neurochemical detection. The microfibers presented here are sensitive, exhibit fast electron transfer, enhanced redox cycling, resist chemical fouling, and maintain frequency independent behavior, similarly to CNT-based material.^{36,3}

METHODS

Chemical/Reagents. All chemicals were purchased from Fisher Scientific (USA) unless otherwise noted. A Tris buffer (15 mM Tris, 1.25 mM NaH₂PO₄, 2.0 mM Na₂SO₄, 3.25 mM KCl, 140 mM NaCl, 1.2 mM CaCl₂ dehydrate, and 1.2 mM MgCl₂) at pH 7.4 was used in all flow injection analysis experiments. Dopamine (DA), norepinephrine (NE), serotonin (5-HT), adenosine (AD) and guanosine (GN) was dissolved in a 0.1 M HCl solution to make 10 mM stock solutions (Sigma-Aldrich, St. Louis, MO, USA), and the solutions were stored at 4 °C. Stock solutions were diluted daily in Tris buffer for experiments. Single-layer graphene oxide dispersion in water (10 mg,mL, ACS material, Pasadena, CA) and L-ascorbic acid 99% (Vitamin C) was purchased from Sigma-Aldrich. All aqueous solutions were made from deionized water (Milli-Q, Millipore, Billerica MA). Artificial cerebrospinal fluid (aCSF) was used for all brain slice experiments and consisted of 2.5 mM KCl, 1.2 mM NaH2PO4, 2.4 mM CaCl2 dihydate, 1.2 mM MgCl₂

hexahydrate, 126 mM NaCl, 11 mM D-glucose, 25 mM sodium bicarbonate, and 0.4 mM ascorbic acid.

GO and rGO Microfiber Fabrication. A hydrothermal method was used to synthesize GO and rGO microfibers. A solution of 10 mg/mL GO dispersions in water with 1 w/w % L-ascorbic acid was mixed together and injected into a glass capillary tube (1 \times 0.25 mm; A&M Systems, Inc., Seqium, WA, USA). Air-dry expoxy (J-B Weld 50112 ClearWeld Quick-Setting Epoxy Syringe - Clear) was used to seal the ends of the glass capillaries. The glass capillary was placed in an oven set to 80 °C for 2 h to produce GO microfibers. To synthesize rGO microfibers, the oven was set to 280 °C for 1 h because between 200 and 300 °C, GO will reduce to rGO. To release the fiber from the capillary, the epoxy was removed and the tube was placed in isopropyl alcohol to easily extract the microfibers.

Microelectrode Fabrication. Graphene fibers were used to construct disk GO or rGO microelectrodes. Briefly, graphene fibers were vacuum aspirated into a glass capillary tube (1.2×0.68 mm, A&M Systems, Inc., Sequim WA, USA) and pulled using a vertical Narishige PE-22 electrode puller (Tokyo, Japan). Graphene fibers were cut near the glass seal under a microscope (Fisher Education). Electrodes were sealed with Epoxy Resin 828 with 14% (w/w) 1,3-phenylenediamine (Sigma-Aldrich) in a 80–85 °C water bath and the electrodes were washed in acetone for about 3 s to removing from excess epoxy. The epoxied electrodes were cured at 100 °C overnight. All electrodes were polished by a fine diamond abrasive plate set to 45° to create a polished disk microelectrode. Electrodes were soaked in isopropyl alcohol for at least 10 min prior to use and backfilled with 1 M KCl.

Electrochemical Detection Methods. Fast-scan cyclic voltammograms were collected using the WaveNeuro potentiostat (Pine Instruments, Durham, NC, USA). Data was collected using a National Instruments PCIe-6363 interface board (Austin, TX, USA) and HDCV software (UNC-Chapel Hill, Mark Wightman). Cyclic voltammograms (CVs) were background subtracted to remove nonfaradaic currents. The electrode was scanned from −0.4 to 1.3 V (vs Ag/AgCl) and back with a 400 V/s scan rate and a repetition rate of 10 Hz. The electrode was equilibrated for 10 min prior to testing, and the average current for each analyte was recorded. Electrodes were tested using a home-built flow injection analysis system using a six-port HPLC actuator (Valco Instruments, Houston, TX, USA). A syringe pump (Chemyx, Stafford, TX, USA) set to a flow rate of 1 mL min⁻¹ was used to deliver buffer and sample to the electrode. All experiments were performed at room temperature. Cyclic voltammetry experiments were performed with a CHI 620 potentiostat (CH Instruments, Bee Cave, TX, USA). A three electrodes system was used where the working electrode was the disc graphene microfiber electrode: GO, and rGO microelectrode. The reference electrode was a standard Ag/ AgCl electrode, and the counter electrode was a Pt wire.

Surface Characterization. The physical and chemical properties of the graphene microfibers were assessed using standard surface characterization techniques. To visualize and qualitatively assess the electrode and individual fibers, scanning electron microscopy (SEM) micrographs were collected using an FEI XL30 SEM. Raman spectra of the fibers were collected using a Renishaw InVia Raman microscope (Guocestershire, UK) excited by a 633 nm Ar-ion laser at 10% power. X-ray photoelectron spectroscopy (XPS, Axis HSi 165 Ultra by

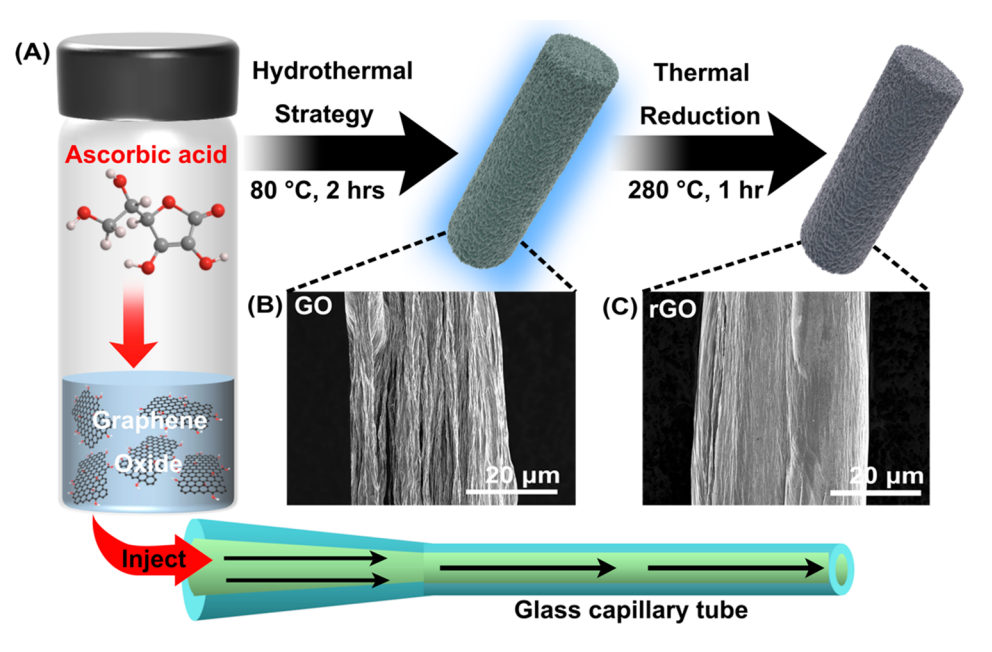


Figure 1. Hydrothermal method used to synthesize GO and rGO microfibers. (A) Schematic representation of the process. (B) SEM image of a GO microfiber. (C) SEM image of a rGO microfiber.

Kratos) was used to measure the chemical composition of the surface. The X-ray source was operated at 12 kV and 10 mA emission.

Endogenous Dopamine Detection in Brain Slices. All animal procedures were conducted according to the National Research Council's The Guide for the Care and Use of Laboratory Animals ("The Guide") and followed guidelines set by the Institutional Animal Care and Use Committee (IACUC) at the University of Cincinnati. Male Sprague-Dawley rats weighing 165-180 g (Charles River Laboratories, Wilmington, MA, USA) were provided food and water ad libitum and housed in a vivarium. Rats were anaesthetized with isofluorane (Henry Shrein, Melville, NY, USA) prior to surgery and euthanized via decapitation immediately before the experiment. The brain was excised and chilled for 2 min in ice-cold oxygenated (5% CO₂, 95% O₂) aCSF. The brain hemispheres were separated by a scalpel and mounted on the vibratome stage with superglue for slicing. Coronal slices of the caudate putamen, 400 μ m thick, were collected with a VT1000S vibratome (Leica, Chicago, IL, USA) set to a frequency of 3 and speed of 90. Slices recovered undisturbed in oxygenated aCSF for 1 h before beginning experiments.

For the collection of dopamine transients, slices were perfused in oxygenated aCSF at 2 mL min⁻¹ with a Watson-Marlow 205S peristaltic pump (Wilmington, MA, USA) at 37 °C in a controlled-temperature chamber (Holliston, MA, USA). A carbon-fiber microelectrode was implanted approximately 75 μ m deep with a micromanipulator (Narishige, Tokyo, Japan). The electrode was equilibrated for approximately 10 min before data was recorded. Dopamine release was recorded from the electrode. Endogenous signaling events were successfully detected in four slices.

Statistics. All data were analyzed with GraphPad Prism V. 9.0 (GraphPad Software Inc., La Jolla, CA, USA). Statistical p-values were significant at 95% confidence level (p < 0.05). Values are reported as the mean \pm standard error of the mean (SEM), and n represents the number of electrodes or slices.

The XPS data were analyzed by peak fit in OriginLab 2019b (OriginLab, Northampton, MA, USA).

RESULT AND DISCUSSION

Graphene-Based Microfiber Synthesis and Characterization. Graphene-based fibers were synthesized using a modified hydrothermal strategy to produce approximately 20-30 μ m microfibers (Figure 1). The hydrothermal method is an effective method to fabricate three-dimensional graphene structures by using heat to promote increases in the π - π interaction between the graphene sheets to help assemble fibers. 25,38 This method usually recommends temperatures of more than 230 °C;²⁶ however, Li et al. introduced the concept of adding L-ascorbic acid to enhance interaction between GO sheets, which enabled the use of only 80 °C to fabricate graphene fibers. 39,40 Here, we used a 10 mg/mL GO dispersion mixed with 1 w/w % L-ascorbic acid and this suspension was injected into a small glass capillary, sealed, and placed in an over set to 80 °C for 2 h to create GO fibers (Figure 1B). Higher temperatures were used to create rGO fibers (Figure 1C). Fibers were removed from the glass capillary and used to make disk microelectrodes (Figure S1). Small voids across the fiber surface were observed in all electrodes, which can result in slight variations in the absolute surface area of each electrode. Despite this observation, batch to batch fabrication was fairly reproducible as demonstrated by the relatively low error in observed oxidative current across all electrodes reported. The detailed surface characterization of GO and rGO microelectrodes is presented in Figure 1A, followed by a detailed electrochemical characterization using both slow scan and fast-scan cyclic voltammetry.

Surface Characterization. *X-ray Photoelectron Spectroscopy (XPS).* Graphene fibers were analyzed with XPS to quantitate the degree of oxygen functionality on the surface before and after thermal reduction. Oxide functionality is important for enhancing adsorption of neurochemical analytes like catecholamines on the carbon surface for sensitive detection. Ascorbic acid (AA) was used to facilitate

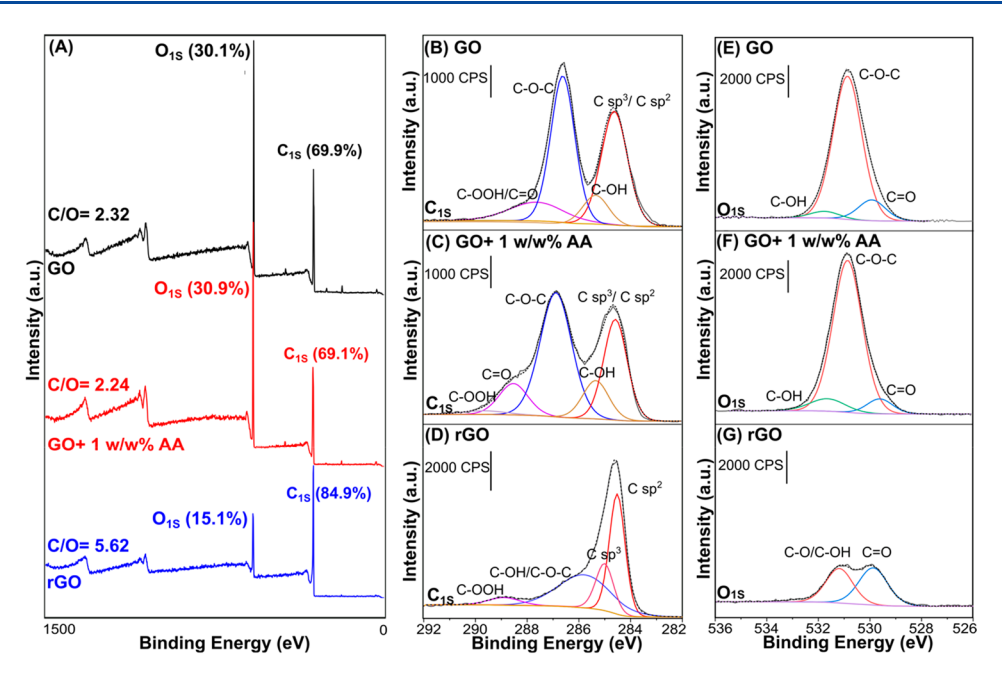


Figure 2. Oxygen content on GO fibers is significantly impacted by the thermal reduction but not by the addition of low weight percent ascorbic acid. (A) XPS survey spectra of GO fibers synthesized without ascorbic acid (black), with 1 w/w % L-ascorbic acid (red), and thermally reduced rGO fibers (blue). (B–G) Deconvoluted C 1s and O 1s peaks for GO (B,E), GO+1 w/w % ascorbic acid (C,F), and rGO (D,G).

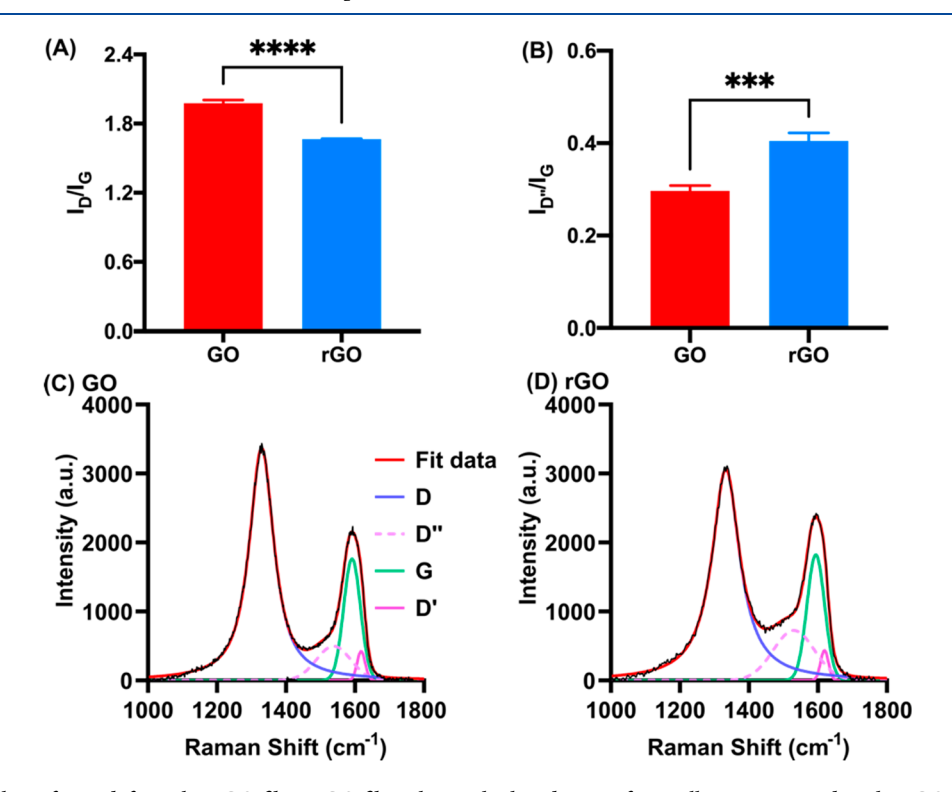


Figure 3. rGO fibers have fewer defects than GO fibers. GO fibers have a higher degree of crystallinity compared to the rGO fibers. (A) $I_{\rm D}/I_{\rm G}$ ratio values for GO and rGO are significantly different (unpaired t test, p < 0.0001, n = 6). (B) $I_{\rm D''}/I_{\rm G}$ ratio is significantly less for GO compared to rGO fibers (unpaired t test, p < 0.001, n = 6). Peaks were further analyzed to reveal the abundance of D'' and D' for both GO (C) and rGO (D).

interactions between the GO sheets to assist in fiber assembly. AA is a known reducing agent, and so comparisons of the XPS spectra for GO without AA, GO with 1 w/w % AA, and rGO with 1 w/w% AA were made to ensure that we could technically label the fibers that were not thermally reduced, "GO" (Figure 2). It is important to note that making fibers without using a "binder" like AA is extremely difficult,

especially at this size scale and therefore was necessary to produce robust, yet small microfibers. The overall XPS spectra for each graphene-based material were superimposed, and the results are plotted in Figure 2A for comparison. The two peaks analyzed were C 1s and O 1s. On average, adding 1 w/w % AA to the GO suspension did not significantly change the weight percentage of C 1s and O 1s elements. The C/O for GO fibers

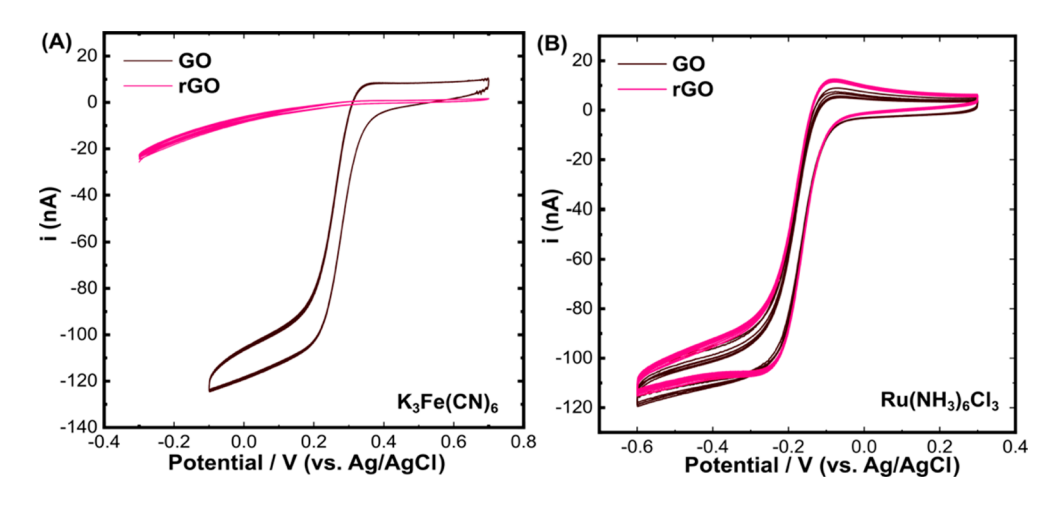


Figure 4. Graphene-based fibers have different electrochemical behavior with surface sensitive vs surface insensitive analytes with traditional cyclic voltammetry. (A) Example CV profiles of equimolar 5 mM of $K_3[Fe(CN)_6]$ dissolved in 1.0 M KCl solution at graphene oxide (GO) and reduced graphene oxide (rGO) at a scan rate of 50 mV/s. (B) Example CV of $Ru(NH_3)_6Cl_3$ in aqueous solution at a GO and rGO at a scan rate of 50 mV/s.

without AA is 2.32 and is 2.34 with the addition of AA. This demonstrates that this low percent AA is not significantly impacting the surface chemistry. In comparison, when we added 10 w/w % AA, we observed a larger loss in oxygen functionality on the surface (Figure S2). Because of these results, we maintain that AA is necessary for helping increase π - π interactions for forming robust fibers yet similar amounts of oxygen are still present on the fiber surface when using low weight percent AA. Because of this, we have chosen to label fibers that were not thermally reduced as "GO fibers". Curve fitting at specific bonding energies was done to identify individual functional groups (Figure S2B-G). The C 1s graphitic peak centers at 284.6 eV (Figure 2B-D). In addition, the C-O peak is centered at 285.5-286.1 eV, the C=O at 287 eV, and the O—C=O peak is at 289 eV (Figure 2B-D). The O 1s peaks are centered at 531-531.4 eV (-C=O), 532.1-533 eV (C-O), and 534 eV (C-OH) (Figure 2E-G). Analysis of these different functional groups reveals significant differences between GO and rGO fibers. The oxygen content on the rGO was only 15.1%, compared to 30.1% on the GO fiber. This demonstrates a reduction in oxygen content by 2-fold after thermal reduction, providing evidence that these two fibers (GO and rGO) are different chemically.

Raman Spectroscopy. Raman spectroscopy is a common experimental technique used to characterize sp² and sp³ carbon and to elucidate the structure of carbon-based materials. 41-44 The Raman spectra of graphene fibers are different than typical carbon fibers (Figure S3A). Both GO and rGO have a 2D band (~2700 cm⁻¹), and this peak is not observed on traditional PAN-based carbon fiber. The D (~1350 cm⁻¹) and 2D bands demonstrate the presence of defects on the material, and surface oxidation can affect these bands. 43,45 The G band is centered at ~1580 cm⁻¹ and represents graphitic carbon. The bare carbon fiber's D/G area under the curve ratio is 1.88 ± 0.14 (Figure S3B, n = 5), similar to prior reports. ^{10,46,47} The D/G area under the curve ratio decreased to 1.69 \pm 0.06 for GO and 1.68 \pm 0.14 for rGO fibers (Figure S3B). The changes in surface defects are not significantly different between the bare carbon fiber and graphene-based material (One-way ANOVA, Bonferroni post-test, p = 0.4765, n = 5). To further

analyze these peaks, we took the ratio of the intensity of the D and G peaks $(I_{\rm D}/I_{\rm G})$. GO's $I_{\rm D}/I_{\rm G}$ is 1.98 \pm 0.03, and rGO is 1.67 \pm 0.004, and these ratios are significantly different (Figure 3A, unpaired t test, p < 0.0001, n = 6). This analysis of the D and G peaks is much more common in the literature compared to analyzing the area under the curve. This result demonstrates differences in the level of defects on the GO and rGO surface. To better understand the graphene-based material's surface structure, additional Raman peak analysis was performed to identify surface defects.

The ratio of the intensity of the D band with the G band (I_D/I_G) is commonly used to estimate the degree of defects on carbon-based material; however, in graphene-based materials, the G peak is the superposition of multiple peaks. 44,48 Therefore, only analyzing the intensity ratio between the D and the G peaks is unreliable. Claramunt et al.48 and King et al. 43 discovered that the G peak is a superposition of the G and D' peaks. According to this understanding, we used peak fitting to analyze these peaks further (Figure 3C-D). We reveal the presence of the following four reported bands in the region between 1000 and 1800 cm⁻¹: D, D", G and D'. This result is important for the analysis of the D-G band for GO and rGO. The D' band appears at ~1635 cm⁻¹ and D" band at 1500-1550 cm⁻¹, and these two peaks provide information about the oxygen content. The shift in the D" position and the intensity ratio of D" and G can indicate oxygen content to estimate the degree of graphene-oxide reduction. 41,48,49 The $I_{D''}/I_G$ ratio is used to estimate the degree of crystallinity: the ratio increases as the crystallinity decreases. Likewise, the crystallinity is proportional to the degree of defects. The $I_{\mathrm{D''}}/I_{\mathrm{G}}$ ratio for GO fibers is 0.30 ± 0.01 and is significantly different than that of rGO (0.40 \pm 0.02, Figure 3B, unpaired *t* test, *p* < 0.001, *n* = 6). This result indicates that the level of crystallinity of GO is higher than that of rGO. Not only are the intensities important, but a shift in the D" peak can indicate changes in the oxygen content: when oxygen content decreases, the peak shifts from higher to lower wavenumbers. 48 For GO fibers, the D" peak appears at \sim 1525 cm⁻¹ and it shifts to \sim 1516 cm⁻¹ for rGO fibers (Figure 3C,D). The Raman data directly supports the XPS data, which suggests that oxygen content is reduced at the rGO fibers. Overall, the comprehensive Raman

analysis provides further insight into the crystallinity, oxygen content, and degree of defects on the GO and rGO microfiber surfaces.

Electrochemical Characterization. Traditional cyclic voltammetry along with outer- $(Ru(NH_3)_6^{3+/2+})$ and inner-sphere (Fe(CN)₆^{3-/4}) redox couples were used to characterize the basic electrochemical performance of the GO and rGO microelectrodes. The electron transfer kinetics for Ru-(NH₃)₆^{3+/2+} are primarily sensitive to the density of the electronic states, and remains insensitive to the surface chemistry.⁵⁰ On the other hand, the $Fe(CN)_6^{3-/4}$ redox probe is sensitive to both surface chemistry and electronic properties, as well as surface cleanliness. 51 Figure 4 shows cyclic voltametric i-E curves for 5 mM Ru(NH₃)₆^{3+/2+} and $Fe(CN)_6^{3-/4-}$ in 1 M KCl recorded at 50 mV/s at (A) GO and (B) rGO microelectrodes. Well-defined, sigmoidal curves were observed for both redox couples at the GO microelectrode. Additionally, the oxidation and reduction peak currents increased linearly with the square root of scan rate (not shown), suggesting diffusion-controlled interactions. The peak potential separation, $\Delta E_{\rm p}$, at GO microelectrodes was 127.3 \pm 5.7 and 135.1 \pm 4.5 mV for Ru(NH₃)₆^{3+/2+} and Fe(CN)₆^{3-/4}, respectively. However, the electrochemical performance of the rGO microelectrodes showed significantly different behavior. While the i-E curves for $Ru(NH_3)_6^{2+/3+}$ remained unchanged in shape and the peak potential separation ($\Delta E_p = 132 \pm 4.2$ mV), no distinguishable redox peaks for Fe(CN)₆^{3-/4-} were observed. This indicates that the chemical structure of the GO and rGO fibers are different, and that $Fe(CN)_6^{3-/4-}$ detection is dependent on the level of defects. Additionally, we speculate that the observed contrast in the electrochemical performance might be attributed to differences in structural disorder between both GO and rGO fibers.

Fast-Scan Cyclic Voltammetry (FSCV). Fast-scan cyclic voltammetry (FSCV) is an electroanalytical technique used to study subsecond fluctuations of neurotransmitters in the brain. We used the "traditional" dopamine waveform for these studies, which starts at a holding potential of -0.4 V and ramps to a switching potential of 1.3 V at a scan rate of 400 V/s. Example data for 1 µM dopamine at both GO and rGO microfibers is shown in Figure 5. Dopamine was chosen due to its popularity with FSCV detection and predictable interactions at carbon-based materials. Example false color plots for both GO and rGO fibers demonstrate detection of dopamine at graphene-based microfiber surfaces (Figure 5A,B). Example dopamine cyclic voltammograms (CVs) for GO, rGO, and bare carbon fibers demonstrate changes in the $\Delta E_{\rm p}$ and redox cycling for dopamine (Figure 5C). On average, we observe significantly faster electron transfer kinetics, as indicated by a smaller $\Delta E_{\rm p}$ at both GO and rGO microfibers, compared to bare carbon fibers (One-way ANOVA, p = 0.0064, n = 8-15, Table 1). GO is significantly different compared to traditional carbon fiber (One-way ANOVA, Bonferroni, p = 0.0053, n =8-15). In addition to faster electron transfer kinetics, we observe enhanced redox cycling at graphene-based surfaces. To quantitate this, we calculated the ratio of the reduction current to oxidation current for dopamine, I_r/I_0 (Table 1) for the GO, rGO, and bare carbon fiber. A value closer to 1.0 indicates 100% reversibility. It is important to note that faster electron transfer and enhanced redox cycling is observed at GO compared to rGO fibers, likely due to the reduction in oxide functionality at the surface which is known to be important for dopamine adsorption and electrocatalytical behavior. Overall,

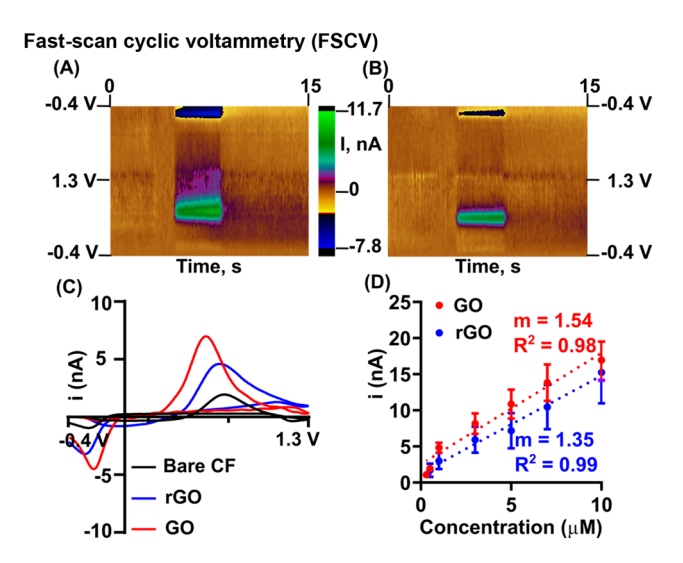


Figure 5. Detection of dopamine at graphene-based microfibers with FSCV. (A and B) Example false color plot for 1 μ M DA at GO and rGO fibers with FSCV. (C) Example CV for dopamine at traditional, bare carbon fibers (black), GO fibers (red), and rGO fibers (blue) demonstrating improvements in electron transfer and redox cycling. (D) Current vs concentration curve for dopamine at GO (red) and rGO (blue) fibers. Slope and R^2 values are shown on the plot.

these findings indicate that graphene-based materials are advantageous for dopamine detection and have superior properties compared to traditional carbon-fiber electrodes.

The sensitivity and limit of detection for dopamine was determined at both GO and rGO disk microelectrodes. On average, the sensitivity for dopamine at GO microelectrodes was $1.54 \pm 0.5 \text{ nA}/\mu\text{M}$ (n = 10) and $1.35 \pm 0.4 \text{ nA}/\mu\text{M}$ for rGO (n = 7) when observing the slope of the concentration curve ranging from 300 nM to 10 μ M. The sensitivity at bare disk carbon-fiber microelectrodes is only 0.41 \pm 0.09 (Figure S4, n = 5); however, it is important to note that disk CFME's are about half the size of disk GF microelectrodes, which makes direct comparison of their sensitivities difficult. Likewise, the limits of detection for dopamine at disk GO, rGO, and CF microelectrodes are 61.1 \pm 1.4 nM, 68.6 \pm 2.3 nM, and 185.2 ± 10.4 nM, respectively. Lower concentrations of DA can be detected at disk graphene-based microelectrodes compared to CFME's. This could be potentially useful in the future because most in vivo studies are conducted at cylindrical CFME's due to the significant loss of sensitivity at disk CFME's. The ability to use disk microelectrodes in tissue would significantly improve the spatial resolution of the measurement.

Adsorption-limited interactions are maintained for dopamine at both GO and rGO microelectrodes. To determine the interaction of 1 μ M dopamine at GO and rGO surfaces, the oxidative peak current was analyzed as a function of scan rates ranging from 50 to 1000 V/s. The log of the oxidative current vs the log of the scan rate helped identify the dominant interaction at the electrode surface (Figure S5, n = 4-5). A slope closer to 1.0 indicates an adsorption-controlled process and a slope closer to 0.5 indicates a diffusion-limited process. It is well-established that dopamine is adsorption-limited at carbon-fiber surfaces. Overall, we observe a slope of 0.9522 for GO, and a slope of 0.9030 for rGO indicating adsorption-limited processes for dopamine at both surfaces.

Table 1. Graphene-Based Materials Exhibit Superior Properties Compared to Traditional Carbon-Fiber Microelectrodes

| material | D/G ratio | $\Delta E_{ m p,DA} m (V)$ | $I_{ m r}/I_{ m o}$ | sensitivity to DA ($nA/\mu M$) | $LOD_{DA}\ (nM)$ |
|---------------|-----------------|-----------------------------|---------------------|----------------------------------|--------------------|
| GO fibers | 1.69 ± 0.06 | 0.87 ± 0.01^a | 0.77 ± 0.04^{b} | 1.54 ± 0.50 | 61.1 ± 1.4^{b} |
| rGO fibers | 1.68 ± 0.14 | 0.91 ± 0.02 | 0.73 ± 0.04^{b} | 1.35 ± 0.40 | 68.6 ± 2.3^{b} |
| carbon fibers | 1.88 ± 0.14 | 0.96 ± 0.02 | 0.39 ± 0.01 | 0.41 ± 0.09 | 185.2 ± 10.4 |
| 2 1 | , | | | | |

^ap < 0.01. ^bp < 0.0001 (One-way ANOVA, Bonferroni post-tests).

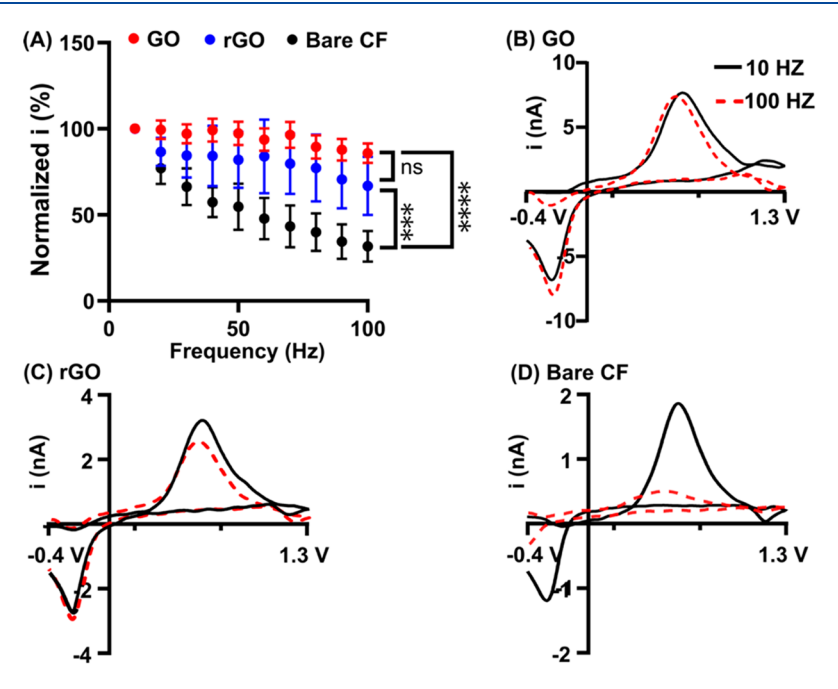


Figure 6. Faster frequency measurements are capable at GO and rGO fibers compared to bare carbon fibers. (A) Frequencies ranging from 10 to 100 Hz were tested. Current is normalized to 10 Hz and plotted as a function of frequency. Normalized current for bare carbon fiber is significantly lower at 100 Hz than both GO and rGO (One-way ANOVA, Bonferroni post-test, p < 0.0001, n = 10). Example CV's for dopamine at 10 and 100 Hz for GO (B), rGO (C), and bare CF (D) demonstrate the loss in signal at higher frequencies for traditional CFME's.

Faster Temporal Resolution Capabilities at Graphene Microelectrodes. Carbon nanomaterials including carbon nanotube yarns and nanospikes have demonstrated "frequency independent" behavior for catecholamines with FSCV. 17,36 Typical waveforms for FSCV are applied at a 10 Hz frequency providing its characteristic 100 ms temporal resolution. Increasing the waveform application frequency leads to decreases in the time between scans (holding time), which ultimately leads to less time for preconcentration of dopamine on the electrode surface causing decreases in sensitivity at higher frequencies for traditional carbon fibers (Figure 6A black and Figure 6D). The Venton group discovered that this frequency dependent behavior does not exist at carbon nanomaterial-based and cavity carbon nanopipette electrodes.^{17,36} This has been hypothesized to be due to local trapping of dopamine in the crevices on the carbon nanomaterial surface. Here, we demonstrate that we observe the same phenomena at graphene-based microelectrodes (Figure 6). The oxidative current for dopamine was analyzed and normalized to the current for 10 Hz. Frequencies ranging from 10 to 100 Hz were tested. On average, the oxidative current was reduced by $68.3 \pm 6.7\%$ at 100 Hz for traditional carbon fibers; conversely, the oxidative current decreased only $14.1 \pm 1.6\%$ for GO and $33.1 \pm 2.9\%$ for rGO fibers. No significant differences were observed at 100 Hz for GO and rGO microfibers (One-way ANOVA, Bonferroni post-test, p =0.1601, n = 10). The decrease in current at 100 Hz was

significantly different between carbon fiber and GO (One-way ANOVA, Bonferroni post-test, p < 0.0001, n = 10) and rGO (One-way ANOVA, Bonferroni post-test, p = 0.1225, n = 10). Likewise, we demonstrate no major changes in the shape of the current vs time trace at 10 and 100 Hz (Figure S6). A smaller "decay current" was observed at higher frequencies, which could indicate local trapping of dopamine on the surface leading to slower desorption from the surface. This is an exciting result and demonstrates that faster temporal resolution, up to 10 ms temporal resolution, measurements are likely for dopamine at graphene-fiber microelectrodes. Future work could focus on controlling the 3D surface structure of graphene fibers to investigate fundamental changes in frequency dependent behavior.

Antifouling Behavior for Graphene-Based Microfibers. Our lab and others have investigated the fouling-resistant behavior of carbon-nanotube fibers. 8,10,16,20,52 Serotonin (5-HT) is an important neurotransmitter in the brain and often detected with FSCV; 6,8,53 however, serotonin is known to polymerize and foul the electrode surface. 6,54,55 The use of carbon nanomaterial-based electrodes have enabled improved stability of serotonin detection due to the incredible fouling-resistant behavior of carbon nanomaterials. Here, we compared the extent to which GO and rGO microelectrodes resist serotonin fouling compared to traditional CFME's (Figure 7). To test the extent to which graphene-based microelectrodes resist fouling, 1 μ M serotonin and 1 μ M

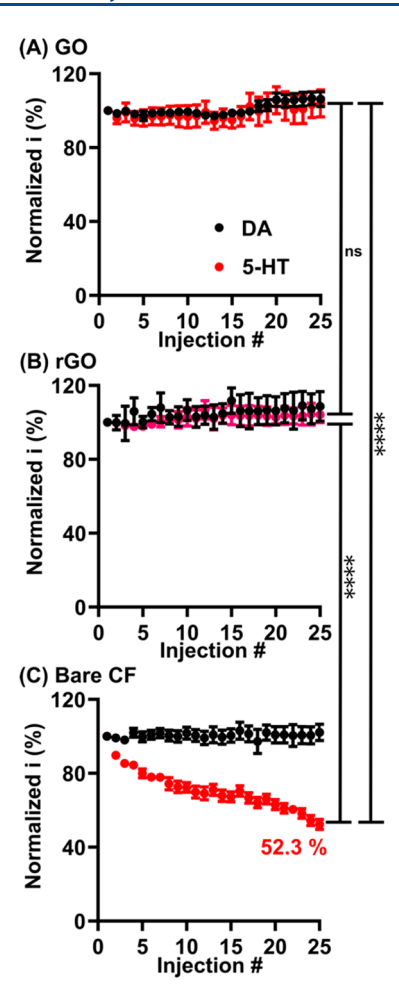


Figure 7. Fouling resistant behavior is observed for GO and rGO microfibers. 1 μ M serotonin was repeatedly injected at the electrode 25×. The oxidative current for serotonin was normalized to the first injection and plotted as a function of injection number for GO (A), rGO (B), and bare carbon fiber (C). Significant loss in current is observed for serotonin at the 25th injection for bare CF compared to GO and rGO (One-way ANOVA, Bonferroni, GO compare with Bare cabon fiber, p < 0.0001, n = 9; rGO compare with bare cabon fiber, p < 0.0001, n = 8).

dopamine were repeatedly injected at the electrode surface, and their oxidative current was monitored over time, similar to previous reports.^{8,10,20} Low concentrations of dopamine do not foul carbon fibers with FSCV and is therefore used as a control (Figure 7, black symbols). On average, a loss of $52.3 \pm 2.2\%$ in the serotonin signal was observed by the 25th injection for CFME's and only a loss of $2.8 \pm 0.3\%$ for dopamine (Figure 7C, n = 10). The normalized percent current for GO and rGO for serotonin at the 25th injection was $103.2 \pm 0.6\%$ and 104.1 \pm 0.4%, respectively. The differences in normalized signal at the 25th injection were not significantly different between the GO and rGO (Figure 7A,B, One-way ANOVA, Bonferroni, *p* = 0.2743); however, the change in normalized current was significantly different between bare CF's and both GO (Oneway ANOVA, Bonferroni, p < 0.0001, n = 9) and rGO (Oneway ANOVA, Bonferroni, p < 0.0001, n = 8). Both GO and rGO electrodes have lower surface defect sites compared to bare CF, and based on prior studies from our lab, 10 is likely contributing to the improved antifouling behavior. Overall, this result further supports the utility of these brand-new

microelectrode materials and provides direct evidence that these materials can stably detect troublesome neurochemicals like serotonin.

Detection of Other Important Electroactive Neurochemicals with FSCV. Graphene-based electrodes are excellent candidate materials for detection of other important electroactive neurochemicals.⁵⁶ In this study, we show that graphene-based materials are also advantageous materials for serotonin (5-HT), norepinephrine (NE), adenosine (AD), and guanosine (GN) detection (Figure S7). It is important to note that during fabrication, some pores on the graphene-fiber surface are evident. Similar to prior work with CNT-based fibers that demonstrate crevices/pores, we observed enhanced catecholamine cyclization on some of the fibers tested. 16,36,57 Cyclization is evident by observing an extra oxidation peak at approximately 1.16 V, compared to the CV traditionally observed at carbon-fiber microelectrodes (Figure S7E black trace). An example of this observation is demonstrated for norepinephrine detection at a rGO fiber (Figure S7E). Future studies should consider optimizing the porosity of the fiber to further study catecholamine cyclization and to test the extent to which pores impact frequency independent behavior. In addition to catecholamine detection, we observe excellent detection of serotonin. Serotonin is historically difficult to detect at bare carbon fibers due to fouling and low sensitivity using the traditionally used "Jackson waveform" for serotonin detection; 8,58,59 however, we highlight here that high currents are observed for serotonin detection at graphene-based materials and the detection is stable (Figure 7), so modified waveforms are unnecessary. An additional observation when testing other neurochemical analytes is enhanced peaks for the secondary and even tertiary reaction (for adenosine) for purine-based neurochemicals (Figure S7C,D,G,H). Shifts in the peak placement for purines are also observed compared to traditional carbon fibers. On traditional carbon-fiber electrodes, the secondary oxidation peak for purine nucleosides is much smaller and the tertiary peak for adenosine is hardly ever detected.60-62 We have previously observed enhanced secondary and tertiary peaks for purines on metal nanoparticle modified carbon surfaces; however, here we demonstrate that improved electrocatalytic behavior is evident on graphene fibers, eliminating the need to modify the surface with metal nanoparticles.63

Dopamine Detection Ex Vivo with Graphene-Fiber Microelectrodes. Endogenous dopamine was detected in the caudate putamen using GO microelectrodes to demonstrate proof-of-concept use for measurement in tissue. Transient dopamine is commonly measured at carbon-fiber electrodes in the striatum, and we have demonstrated transient dopamine signaling in ex vivo preparations. 64-67 Here, we monitored spontaneous, endogenous dopamine release in the caudate putamen as previously reported. Measurements were made for at least 20 min per slice. Figure 8 demonstrates example data (n = 4 slices in total tested). Slight shifts in peak potential are commonly observed during tissue measurements and is observed here. 64,68,69 Interestingly, a near reversible behavior is still observed in tissue with a I_r/I_o of 0.81, similar to in vitro data (Table 1). This data demonstrates that the GO electrodes are sensitive to analytes in a tissue matrix and suitable for use in biological settings.

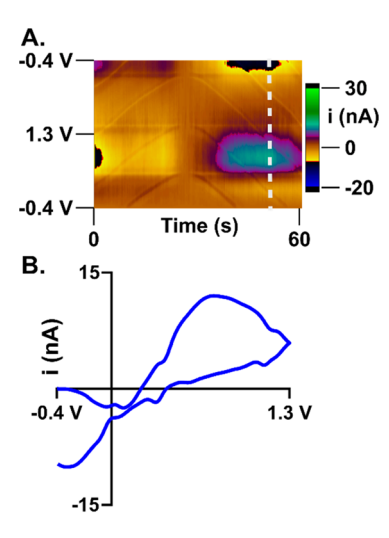


Figure 8. Representative data for endogenous dopamine release detected in slices of the caudate putamen. (A) 3D color plot represents voltage on the *y*-axis, time on the *x*-axis, and current shown in false color. (B) Representative CV for DA.

CONCLUSIONS

Overall, we demonstrate significantly improved detection capabilities using graphene microfibers for FSCV detection. These fibers can be easily synthesized in any standard research laboratory, which we anticipate will improve their accessibility to researchers who are interested in using novel carbon-based materials with excellent electrochemical properties. Importantly, the ability to fabricate both GO and rGO fibers enables fine-tuning of the electrodes' chemical properties that consequently affects their electrochemical behavior and this is dependent on the analyte of interest. This is particularly crucial for any future studies focused on specific analytes, beyond dopamine. We demonstrate here that changes in the electrochemical behavior for dopamine is evident on GO vs rGO fibers: namely, the electron transfer rate and redox cycling behavior. We speculate that the oxide functionality is contributing, in part, to these changes in electrochemical behavior for dopamine; however, others have suggested that disordered carbon is not a prerequisite for fast, reversible kinetics under diffusion-limited conditions.⁷⁰ Because dopamine is adsorption-limited at fast scan rates, our work provides further evidence that under adsorption-limited conditions, oxide functionality is important for improved electrochemical performance. In addition to dopamine voltammetry, we briefly show changes in the electrochemical behavior for other important neurochemical analytes, representing many chemical "classes" including indolamines and purines. Taken together, we provide a strong case for finetuning electrode surfaces based on the analyte of interest. This work also demonstrates that ultrasensitive detection at disk microelectrodes is capable when using graphene-based fibers, which will significantly improve the spatial resolution of analysis in tissue in the future. Lastly, the frequency independent behavior was evident for dopamine at graphene microelectrodes, which expands their potential use for realtime biological sensing, significantly improving FSCV's temporal resolution capabilities.

ASSOCIATED CONTENT

Supporting Information

The Supporting Information is available free of charge at https://pubs.acs.org/doi/10.1021/acs.analchem.1c05637.

SEM image of graphene-oxide fiber microelectrode; XPS analysis of GO mixed with 10 w/w % AA; Raman spectroscopy of graphene-based material and carbon fiber; calibration curve for dopamine; adsorption curve for dopamine at GO and rGO microfibers; example current versus time traces for at GO and rGO microfibers; example CVs for common biological interferents (PDF)

AUTHOR INFORMATION

Corresponding Author

Ashley E. Ross — Department of Chemistry, University of Cincinnati, Cincinnati, Ohio 45221-0172, United States; orcid.org/0000-0003-2456-3636; Email: Ashley.ross@uc.edu

Authors

Yuxin Li — Department of Chemistry, University of Cincinnati, Cincinnati, Ohio 45221-0172, United States Romana Jarosova — Department of Chemistry, University of Cincinnati, Cincinnati, Ohio 45221-0172, United States Moriah E. Weese-Myers — Department of Chemistry, University of Cincinnati, Cincinnati, Ohio 45221-0172,

United States; orcid.org/0000-0003-4836-2142 Complete contact information is available at: https://pubs.acs.org/10.1021/acs.analchem.1c05637

Notes

The authors declare no competing financial interest.

ACKNOWLEDGMENTS

This material is based upon work supported by the National Science Foundation under Grant # 2143520. Any opinions, findings, and conclusions or recommendations expressed in this material are those of the authors and do not necessarily reflect the views of the NSF. The authors also thank the Advanced Materials and Characterization Core at the University of Cincinnati for assistance with collecting the SEM data and the Ohio State University with collecting the XPS data.

REFERENCES

- (1) Bath, B. D.; Michael, D. J.; Trafton, B. J.; Joseph, J. D.; Runnels, P. L.; Wightman, R. M. Anal. Chem. 2000, 72 (24), 5994–6002.
- (2) Huffman, M. L.; Venton, B. J. Analyst 2009, 134 (1), 18-24.
- (3) Bucher, E. S.; Wightman, R. M. Annu. Rev. Anal. Chem. Palo Alto Calif 2015, 8, 239–261.
- (4) Robinson, D. L.; Venton, B. J.; Heien, M. L. A. V.; Wightman, R. M. Clin. Chem. **2003**, 49 (10), 1763–1773.
- (5) Pyakurel, P.; Privman Champaloux, E.; Venton, B. J. ACS Chem. Neurosci. **2016**, 7 (8), 1112–1119.
- (6) Abdalla, A.; Atcherley, C. W.; Pathirathna, P.; Samaranayake, S.; Qiang, B.; Peña, E.; Morgan, S. L.; Heien, M. L.; Hashemi, P. *Anal. Chem.* **2017**, *89* (18), 9703–9711.
- (7) Schmidt, A. C.; Wang, X.; Zhu, Y.; Sombers, L. A. ACS Nano 2013, 7 (9), 7864–7873.
- (8) Swamy, B. E. K.; Venton, B. J. Analyst 2007, 132, 876-884.
- (9) Yang, C.; Wang, Y.; Jacobs, C. B.; Ivanov, I. N.; Venton, B. J. Anal. Chem. **2017**, 89 (10), 5605–5611.

- (10) Weese, M. E.; Krevh, R. A.; Li, Y.; Alvarez, N. T.; Ross, A. E. ACS Sens 2019, 4 (4), 1001–1007.
- (11) Cao, Q.; Hensley, D. K.; Lavrik, N. V.; Venton, B. J. Carbon **2019**, 155, 250-257.
- (12) Cao, Q.; Shao, Z.; Hensley, D. K.; Lavrik, N. V.; Venton, B. J. Langmuir 2021, 37 (8), 2667–2676.
- (13) Shao, Y.; Ying, Y.; Ping, J. Chem. Soc. Rev. 2020, 49 (13), 4405-4465.
- (14) Puthongkham, P.; Venton, B. J. Analyst 2020, 145 (4), 1087-1102.
- (15) Puthongkham, P.; Yang, C.; Venton, B. J. Electroanalysis 2018, 30 (6), 1073–1081.
- (16) Shao, Z.; Puthongkham, P.; Hu, K.; Jia, R.; Mirkin, M. V.; Venton, B. J. *Electrochim. Acta* **2020**, *361*, 137032.
- (17) Yang, C.; Hu, K.; Wang, D.; Zubi, Y.; Lee, S. T.; Puthongkham, P.; Mirkin, M. V.; Venton, B. J. Anal. Chem. **2019**, 91 (7), 4618–4624.
- (18) Yang, C.; Denno, M. E.; Pyakurel, P.; Venton, B. J. Anal. Chim. Acta 2015, 887, 17–37.
- (19) Chang, Y.; Venton, B. J. Anal. Methods **2020**, 12 (22), 2893–2902.
- (20) Zestos, A. G.; Jacobs, C. B.; Trikantzopoulos, E.; Ross, A. E.; Venton, B. J. *Anal. Chem.* **2014**, *86* (17), *8568*–8575.
- (21) Cao, Q.; Puthongkham, P.; Venton, B. J. Anal. Methods 2019, 11 (3), 247–261.
- (22) Kuila, T.; Bose, S.; Khanra, P.; Mishra, A. K.; Kim, N. H.; Lee, J. H. *Biosens. Bioelectron.* **2011**, *26* (12), 4637–4648.
- (23) Huang, Y.; Dong, X.; Liu, Y.; Li, L.-J.; Chen, P. J. Mater. Chem. 2011, 21 (33), 12358-12362.
- (24) Ambrosi, A.; Chua, C. K.; Bonanni, A.; Pumera, M. Chem. Rev. **2014**, 114 (14), 7150–7188.
- (25) Xu, Y.; Shi, G.; Duan, X. Acc. Chem. Res. 2015, 48 (6), 1666–1675.
- (26) Dong, Z.; Jiang, C.; Cheng, H.; Zhao, Y.; Shi, G.; Jiang, L.; Qu, L. Adv. Mater. 2012, 24 (14), 1856–1861.
- (27) Gao, Z.; Zhu, J.; Rajabpour, S.; Joshi, K.; Kowalik, M.lg.; Croom, B.; Schwab, Y.; Zhang, L.; Bumgardner, C.; Brown, K. R.; Burden, D.; Klett, J. W.; van Duin, A. C. T.; Zhigilei, L. V.; Li, X. Sci. Adv. 2020, 6 (17), No. eaaz4191.
- (28) Li, Z.; Xu, Z.; Liu, Y.; Wang, R.; Gao, C. Nat. Commun. 2016, 7 (1), 13684.
- (29) Geim, A. K.; Novoselov, K. S. Nat. Mater. 2007, 6 (3), 183–191.
- (30) Castagnola, E.; Garg, R.; Rastogi, S. K.; Cohen-Karni, T.; Cui, X. T. Biosens. Bioelectron. 2021, 191, 113440.
- (31) Zheng, X.; Hu, Q.; Zhou, X.; Nie, W.; Li, C.; Yuan, N. Mater. Des. 2021, 201, 109476.
- (32) Xu, Z.; Sun, H.; Zhao, X.; Gao, C. Adv. Mater. 2013, 25 (2), 188-193.
- (33) Xin, G.; Zhu, W.; Deng, Y.; Cheng, J.; Zhang, L. T.; Chung, A. J.; De, S.; Lian, J. *Nat. Nanotechnol.* **2019**, *14* (2), 168–175.
- (34) Hofmann, E.; Krüger, K.; Haynl, C.; Scheibel, T.; Trebbin, M.; Förster, S. Lab. Chip 2018, 18 (15), 2225–2234.
- (35) Qing, H.; Ji, Y.; Li, W.; Zhao, G.; Yang, Q.; Zhang, X.; Luo, Z.; Lu, T. J.; Jin, G.; Xu, F. ACS Appl. Mater. Interfaces 2020, 12 (2), 2049–2058.
- (36) Jacobs, C. B.; Ivanov, I. N.; Nguyen, M. D.; Zestos, A. G.; Venton, B. J. *Anal. Chem.* **2014**, *86* (12), 5721–5727.
- (37) Yang, C.; Denno, M. E.; Pyakurel, P.; Venton, B. J. Anal. Chim. Acta 2015, 887, 17–37.
- (38) Xu, Y.; Sheng, K.; Li, C.; Shi, G. ACS Nano 2010, 4 (7), 4324–4330.
- (39) Li, J.; Li, J.; Li, L.; Yu, M.; Ma, H.; Zhang, B. J. Mater. Chem. A 2014, 2 (18), 6359–6362.
- (40) Gao, J.; Liu, F.; Liu, Y.; Ma, N.; Wang, Z.; Zhang, X. Chem. Mater. 2010, 22 (7), 2213–2218.
- (41) Dresselhaus, M. S.; Jorio, A.; Saito, R. Annu. Rev. Condens. Matter Phys. **2010**, 1 (1), 89–108.

- (42) Ferrari, A. C.; Basko, D. M. Nat. Nanotechnol. 2013, 8 (4), 235-246.
- (43) King, A. A. K.; Davies, B. R.; Noorbehesht, N.; Newman, P.; Church, T. L.; Harris, A. T.; Razal, J. M.; Minett, A. I. Sci. Rep. **2016**, 6 (1), 19491.
- (44) Wu, J.-B.; Lin, M.-L.; Cong, X.; Liu, H.-N.; Tan, P.-H. Chem. Soc. Rev. 2018, 47 (5), 1822–1873.
- (45) Pathak, A. K.; Borah, M.; Gupta, A.; Yokozeki, T.; Dhakate, S. R. Compos. Sci. Technol. 2016, 135, 28–38.
- (46) Li, Y.; Fleischer, C. M.; Ross, A. E. Chem. Commun. 2020, 56 (58), 8023–8026.
- (47) Syeed, A. J.; Li, Y.; Ostertag, B. J.; Brown, J. W.; Ross, A. E. Faraday Discuss. **2022**, DOI: 10.1039/D1FD00049G.
- (48) Claramunt, S.; Varea, A.; López-Díaz, D.; Velázquez, M. M.; Cornet, A.; Cirera, A. J. Phys. Chem. C 2015, 119 (18), 10123-10129.
- (49) Muñoz-Ferreiro, C.; López-Pernía, C.; Gallardo-López, Á.; Poyato, R. J. Eur. Ceram. Soc. 2021, 41, 290.
- (50) Chen, P.; McCreery, R. L. Anal. Chem. 1996, 68 (22), 3958–3965.
- (51) McCreery, R. L. Chem. Rev. 2008, 108 (7), 2646-2687.
- (52) Puthongkham, P.; Venton, B. J. ACS Sens 2019, 4 (9), 2403-2411.
- (53) Hashemi, P.; Dankoski, E. C.; Petrovic, J.; Keithley, R. B.; Wightman, R. M. Anal. Chem. **2009**, 81 (22), 9462–9471.
- (54) Hashemi, P.; Dankoski, E. C.; Petrovic, J.; Keithley, R. B.; Wightman, R. M. Anal. Chem. **2009**, 81 (22), 9462–9471.
- (55) Hashemi, P.; Dankoski, E. C.; Lama, R.; Wood, K. M.; Takmakov, P.; Wightman, R. M. *Proc. Natl. Acad. Sci. U. S. A.* **2012**, 109 (29), 11510–11515.
- (56) Zachek, M. K.; Hermans, A.; Wightman, R. M.; McCarty, G. S. J. Electroanal. Chem. Lausanne Switz. 2008, 614 (1–2), 113–120.
- (57) Jacobs, C. B.; Peairs, M. J.; Venton, B. J. Anal. Chim. Acta 2010, 662 (2), 105–127.
- (58) Jackson, B. P.; Dietz, S. M.; Wightman, R. M. Anal. Chem. 1995, 67 (6), 1115-1120.
- (59) Dunham, K. E.; Venton, B. J. Analyst 2020, 145 (22), 7437-7446.
- (60) Swamy, B. E. K.; Venton, B. J. Subsecond Detection of Physiological Adenosine Concentrations Using Fast-Scan Cyclic Voltammetry 2007, 79, 744.
- (61) Swamy, B. E. K.; Venton, B. J. Anal. Chem. 2007, 79 (2), 744–750.
- (62) Cryan, M. T.; Ross, A. E. Analyst 2019, 144 (1), 249-257.
- (63) Li, Y.; Keller, A. L.; Cryan, M. T.; Ross, A. E. ACS Meas. Sci. Au 2021, DOI: 10.1021/acsmeasuresciau.1c00026.
- (64) Regan, S. L.; Cryan, M. T.; Williams, M. T.; Vorhees, C. V.; Ross, A. E. ACS Chem. Neurosci. **2020**, 11, 1171.
- (65) Robinson, D. L.; Heien, M. L. A. V.; Wightman, R. M. J. Neurosci. **2002**, 22 (23), 10477–10486.
- (66) Ariansen, J. L.; Heien, M. L. A. V.; Hermans, A.; Phillips, P. E. M.; Hernadi, I.; Bermudez, M.; Schultz, W.; Wightman, R. M. Monitoring Extracellular PH, Oxygen, and Dopamine during Reward Delivery in the Striatum of Primates. *Front. Behav. Neurosci.* **2012**, *6*. DOI: 10.3389/fnbeh.2012.00036.
- (67) Phillips, P. E. M.; Stuber, G. D.; Heien, M. L. A. V.; Wightman, R. M.; Carelli, R. M. *Nature* **2003**, 422 (6932), 614–618.
- (68) Cryan, M. T.; Ross, A. E. Anal. Chem. 2019, 91 (9), 5987–5993.
- (69) Nguyen, M. D.; Lee, S. T.; Ross, A. E.; Ryals, M.; Choudhry, V. I.; Venton, B. J. *PLoS One* **2014**, *9* (1), No. e87165.
- (70) Martín-Yerga, D.; Costa-García, A.; Unwin, P. R. ACS Sens 2019, 4 (8), 2173-2180.